Self-Assembled Hollow Spheres of β-Ni(OH)$_2$ and Their Derived Nanomaterials

Shengmao Zhang[†] and Hua Chun Zeng*

Department of Chemical and Biomolecular Engineering, Faculty of Engineering, National University of Singapore, 10 Kent Ridge Crescent, Singapore 119260

Received October 21, 2008. Revised Manuscript Received December 25, 2008

This paper describes a novel solution-based chemical process to architect hollow spheres of β-Ni(OH)$_2$ with controllable sizes in submicrometer and micrometer regimes. In the synthesis, starting nickel salt (nitrate) is first converted to 6-coordinated nickel ion complex $[Ni(EDA)_3]^{2+}$ (bidentate ligand EDA = $C_2H_4(NH_2)_2$) to avoid rapid solid formation. Hollow and core−shell β-Ni(OH)$_2$ spheres can be obtained with this template-free approach under one-pot conditions. The β-Ni(OH)$_2$ spheres are constructed from petal-like nanobuilding units which in turn are formed from even smaller nanocrystallites. The obtained porous β-Ni(OH)$_2$ spheres have a large specific surface area and show a unimodal pore-size distribution. Several preparative parameters have been examined and optimized. In particular, the concentration of divalent nickel in the starting solutions plays an important role in controlling thickness of the petal-like β-Ni(OH)$_2$ flakes and diameter of spheres. The β-Ni(OH)$_2$ flakes self-assemble into final spherical products through a donut-like structural intermediate. Furthermore, the β-Ni(OH)$_2$ hollow spheres can be used as solid precursors to synthesize other nanostructured derivatives. In this work, phase pure inorganic nanostructures, carbon nanotube (CNT)−inorganic nanocomposites, and inorganic−inorganic nanocomposites (e.g., NiO, Ni, NiO/Ni, Ni/β-Ni(OH)$_2$, CNTs/NiO, CNTs/Ni, Ni@CNTs, Fe(OH)$_3$/β-Ni(OH)$_2$, Co(OH)$_2$/β-Ni(OH)$_2$, and Mg(OH)$_2$/β-Ni(OH)$_2$) have been prepared via solid-state thermal decomposition, gas-phase reduction, solution-based reduction, surface oxidation, chemical vapor deposition, and liquid-phase deposition. A greater picture for general synthesis of Ni-containing nanomaterials is thus obtained.

1. Introduction

Transition-metal hydroxides are a class of important mineral materials that have many important applications.[1−15] For instance, divalent metal cations (e.g., $M^{II} = Mn^{2+}$, Fe^{2+}, Co^{2+}, Ni^{2+}, Cu^{2+}, Zn^{2+}, etc.) are located in the central spaces of oxygen octahedra formed from six hydroxyl groups. These cation containing octahedra then share their edges to form two-dimensional (2D) sheets similar to the well-known mineral compound brucite Mg(OH)$_2$.[1−6] The resultant 2D sheets can pile up one another along the *c*-axis of brucite crystal via hydrogen bonding among the hydroxyl groups. Intercalation of anions such as nitrates and carbonates to the intersheet space can further take place, which will lead to formation of metal hydroxide salts. For example, while maintaining total charge neutrality, partial substitution of the hydroxyl groups in brucite-like sheets by other anions (e.g., nitrate or carbonate ions) results in expansion of intersheet spacing.[7,8] On the other hand, when some of the divalent cations are oxidized to trivalent ones (e.g., $M^{III} = Cr^{3+}$, Mn^{3+}, Fe^{3+}, Co^{3+}, etc.), both inorganic and organic anions, including negatively charged biomolecules, will be intercalated into the intersheet space to compensate positive charge gain in the oxidation of divalent metal cations. This formation scheme gives rise to another family of metal hydroxides called hydrotalcite-like compounds (HTlcs).[9−15] Apparently, the cause of this intercalation is electrostatic,[9−15] and the alternative stacking of positive-then-negative sheets/layers along the *c*-axis of a rhombohedral crystal symmetry ($R\bar{3}m$) is similar to the natural hydrotalcite compound $Mg_6Al_2(OH)_{16}CO_3 \cdot 4H_2O$.[1−3]

Because of their layered structures, the metal hydroxides tend to form into thin flakes or platelet forms in natural/normal formation environments.[1−15] In view of the rapid

* Corresponding author. Tel: (65) 6516-2896. Fax: (65) 6779-1936. E-mail: chezhc@nus.edu.sg.

[†] On leave from The Key Laboratory of Ministry of Education for Special Functional Materials, Henan University, Kaifeng 475004, China.

(1) Cavani, F.; Trifiro, F.; Vaccari, A. *Catal. Today* **1991**, *11*, 173–301, and references therein.
(2) Vaccari, A. *Catal. Today* **1998**, *41*, 53–71, and references therein.
(3) Rives, V.; Ulibarri, M. A. *Coord. Chem. Rev.* **1999**, *181*, 61–120, and references therein.
(4) Brindley, G. W.; Kikkawa, S. *Am. Mineral.* **1979**, *64*, 836–843.
(5) Xu, Z. P.; Zeng, H. C. *Chem. Mater.* **1999**, *11*, 67–74.
(6) (a) Sampanthar, J. T.; Zeng, H. C. *J. Am. Chem. Soc.* **2002**, *124*, 6668–6675. (b) Cai, F.-S.; Zhang, G.-Y.; Chen, J.; Gou, X.-L.; Liu, H.-K.; Dou, S.-X. *Angew. Chem., Int. Ed.* **2004**, *43*, 4212–4216. (c) Itahara, H.; Seo, W.-S.; Lee, S.; Nozaki, H.; Tani, T.; Koumoto, K. *J. Am. Chem. Soc.* **2005**, *127*, 6367–6373. (d) Liu, Z. P.; Ma, R. Z.; Osada, M.; Takada, K.; Sasaki, T. *J. Am. Chem. Soc.* **2005**, *127*, 13869–13874.
(7) Xu, R.; Zeng, H. C. *Chem. Mater.* **2003**, *15*, 2040–2048, and references therein.
(8) Xu, R.; Zeng, H. C. *Langmuir* **2004**, *20*, 9780–9790.
(9) Cai, H.; Hillier, A. C.; Franklin, K. R.; Nunn, C. C.; Ward, M. D. *Science* **1994**, *266*, 1551–1555.
(10) Choy, J. H.; Kwak, S. Y.; Park, J. S.; Jeong, Y. J.; Portier, J. *J. Am. Chem. Soc.* **1999**, *121*, 1399–1400.
(11) Choy, J. H.; Kwak, S. Y.; Jeong, Y. J.; Park, J. S. *Angew. Chem., Int. Ed.* **2000**, *39*, 4042–4045.
(12) Leroux, F.; Besse, J. P. *Chem. Mater.* **2001**, *13*, 3507–3515.
(13) Xu, Z. P.; Zeng, H. C. *J. Phys. Chem. B* **2001**, *105*, 1743–1749.
(14) Xu, Z. P.; Xu, R.; Zeng, H. C. *Nano Lett.* **2001**, *1*, 703–706.
(15) Allada, R. K.; Navrotsky, A.; Berbeco, H. T.; Casey, W. H. *Science* **2002**, *296*, 721–723.

10.1021/cm8028593 CCC: $40.75
Published on Web 02/02/2009

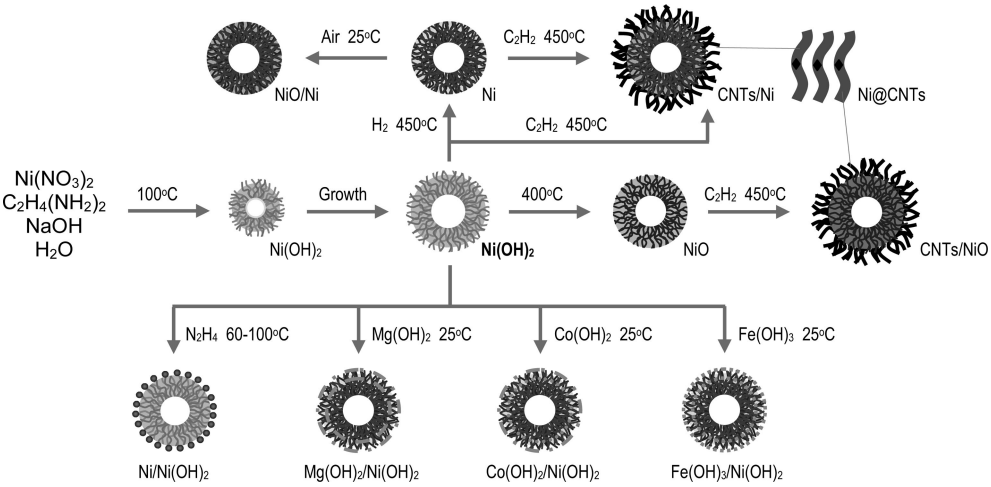

Figure 1. Schematic flowchart for synthesis of hollow spheres of β-$Ni(OH)_2$ and formation processes of their nanostructured derivatives.

development of nanomaterials research over the past decade,[16−21] in addition to the as-formed metal hydroxides, it is highly desirable to organize metal hydroxide flakes or platelets into certain product morphologies for actual applications, such as adding new functionalities and creating interior spaces for inorganic nanostructured materials.[22−40] Because of their low dimension along the [001] axis, moreover, the freestanding layered particles can be viewed as primitive building units for construction of larger architectures.[6,39] This mesoscale organization ensures the assembled materials and their derivatives function as nanomaterials but can be handled in the same ways of conventional bulk materials (e.g., easy separation after use because of larger sizes).[6] In pursuing this research, there have been a number of new synthetic methods proposed in recent years. For example, nickel hydroxide $Ni(OH)_2$ is an important transition metal hydroxide which has been used in a wide range of applications such as rechargeable batteries, heterogeneous catalysis, and so forth.[41−50] As a solid precursor, $Ni(OH)_2$ has also been utilized to derive metallic Ni as well as metal oxide NiO.[44−50] To obtain hierarchical organizations of $Ni(OH)_2$ nanobuilding units, four different solution methods have been developed for this hydroxide. First, solid spherical types of nickel hydroxide [both β-phase and α-phase (a hydrotalcite-like compound)] have been successfully prepared via aggregation of $Ni(OH)_2$ flakes or plaletes.[44,47,50] Second, carnation-like flower structures of brucite-like nickel hydroxide (β-phase) have also been obtained by aggregative growths through different solution routes.[47,49] Third, hollow spheres of nickel hydroxide (β-phase) have been made with assistance of styrene−acrylic acid copolymer (PSA) Latex beads as a growth template.[46] And fourth, hollow spheres of nickel hydroxide (β-phase) have also been obtained after a prolonged hydrothermal treatment at 100−180 °C for 24 h, in which Ostwald ripening is an underlying mechanism for solid evacuation to create central interiors for the spheres.[45] Finally, it should also be mentioned that, because of the importance of Ni-containing materials in various technological applications, nanostructured Ni and NiO have been investigated extensively in recent years.[51−62]

(16) Burda, C.; Chen, X.; Narayanan, R.; El Sayed, M. A. *Chem. Rev* **2005**, *105*, 1025–1102.
(17) Yin, Y.; Alivisatos, A. P. *Nature* **2005**, *437*, 664–670.
(18) Kumar, S.; Nann, T. *Small* **2006**, *2*, 316–329.
(19) Jun, Y.; Chio, J.; Cheon, J. *Angew. Chem., Int. Ed.* **2006**, *45*, 3414–3439.
(20) Park, J.; Joo, J.; Kwon, S. G.; Jang, Y.; Hyeon, T. *Angew. Chem., Int. Ed.* **2007**, *46*, 4630–4660.
(21) Tao, A. R.; Habas, S.; Yang, P. D. *Small* **2008**, *4*, 310–325.
(22) Sun, Y.; Xia, Y. *Science* **2002**, *298*, 2176–2179.
(23) Goldberger, J.; He, R.; Lee, S.; Zhang, Y.; Yan, H.; Choi, H.; Yang, P. D. *Nature* **2003**, *422*, 599–602.
(24) Sun, Y.; Mayers, B.; Xia, Y. *Adv. Mater.* **2003**, *15*, 641–646.
(25) Bao, J.; Liang, Y.; Xu, Z.; Si, L. *Adv. Mater.* **2003**, *15*, 1832–1835.
(26) Peng, Q.; Dong, Y.; Li, Y. *Angew. Chem., Int. Ed.* **2003**, *42*, 3027–3030.
(27) Yang, Z.; Niu, Z.; Lu, Y.; Hu, Z.; Han, C. C. *Angew. Chem., Int. Ed.* **2003**, *42*, 1943–1945.
(28) Nakashima, T.; Kimizuka, N. *J. Am. Chem. Soc.* **2003**, *125*, 6386–6387.
(29) Guo, C.-W.; Cao, Y.; Xie, S.-H.; Dai, W.-L.; Fan, K.-N. *Chem. Commun.* **2003**, 700–701.
(30) Yang, H. G.; Zeng, H. C. *J. Phys. Chem. B* **2004**, *108*, 3492–3495.
(31) Yin, Y.; Rioux, R. M.; Erdonmez, C. K.; Hughes, S.; Somorjai, G. A.; Alivisatos, A. P. *Science* **2004**, *304*, 711–714.
(32) Sun, Y.; Xia, Y. *Adv. Mater.* **2004**, *16*, 264–268.
(33) Yang, H. G.; Zeng, H. C. *Angew. Chem., Int. Ed.* **2004**, *43*, 5206–5209.
(34) Wang, Y.; Lee, J. Y.; Zeng, H. C. *Chem. Mater.* **2005**, *17*, 3899–3903.
(35) Jeong, U.; Wang, Y.; Ibisate, M.; Xia, Y. *Adv. Funct. Mater.* **2005**, *15*, 1907–1921.
(36) Li, J.; Zeng, H. C. *Angew. Chem., Int. Ed.* **2005**, *44*, 4342–4345.
(37) Pan, Y.; Huo, K.; Hu, Y.; Fu, J.; Lu, Y.; Dai, Z.; Hu, Z.; Chen, Y. *Small* **2005**, *1*, 1199–1203.
(38) Liu, B.; Zeng, H. C. *Small* **2005**, *1*, 566–571.
(39) Zeng, H. C. *J. Mater. Chem.* **2006**, *16*, 649–662.
(40) Li, J.; Zeng, H. C. *J. Am. Chem. Soc.* **2007**, *129*, 15839–15847.
(41) Oliva, P.; Leonardi, J.; Laurent, J. F.; Delmas, C.; Braconnier, J. J.; Figlarz, M.; Fievet, F.; de Guibert, A. *J. Power Sources* **1982**, *8*, 229–255.
(42) Liang, Z.-H.; Zhu, Y.-J.; Hu, X.-L. *J. Phy. Chem. B* **2004**, *108*, 3488–3491.
(43) Yang, D. N.; Wang, R. M.; He, M. S.; Zhang, J.; Liu, Z. F. *J. Phys. Chem. B* **2005**, *109*, 7654–7658.
(44) Ni, X. M.; Zhao, Q. B.; Cheng, J.; Zheng, H. G.; Li, B. B.; Zhang, D. G. *Chem. Lett.* **2005**, *34*, 1408–1409.
(45) Wang, Y.; Zhu, Q. S.; Zhang, H. G. *Chem. Commun.* **2005**, 5231–5233.
(46) Wang, D. B.; Song, C. X.; Hu, Z. S.; Fu, X. *J. Phys. Chem. B* **2005**, *109*, 1125–1129.
(47) Cao, M. H.; He, X. Y.; Chen, J.; Hu, C. W. *Cryst. Growth Des.* **2007**, *7*, 170–174.
(48) Orikasa, H.; Karoji, J.; Matsui, K.; Kyotani, T. *Dalton Trans.* **2007**, 3757–3762.
(49) Yang, L.-X.; Zhu, Y.-J.; Tong, H.; Liang, Z.-H.; Wang, W.-W. *Cryst. Growth Des.* **2007**, *7*, 2716–2719.

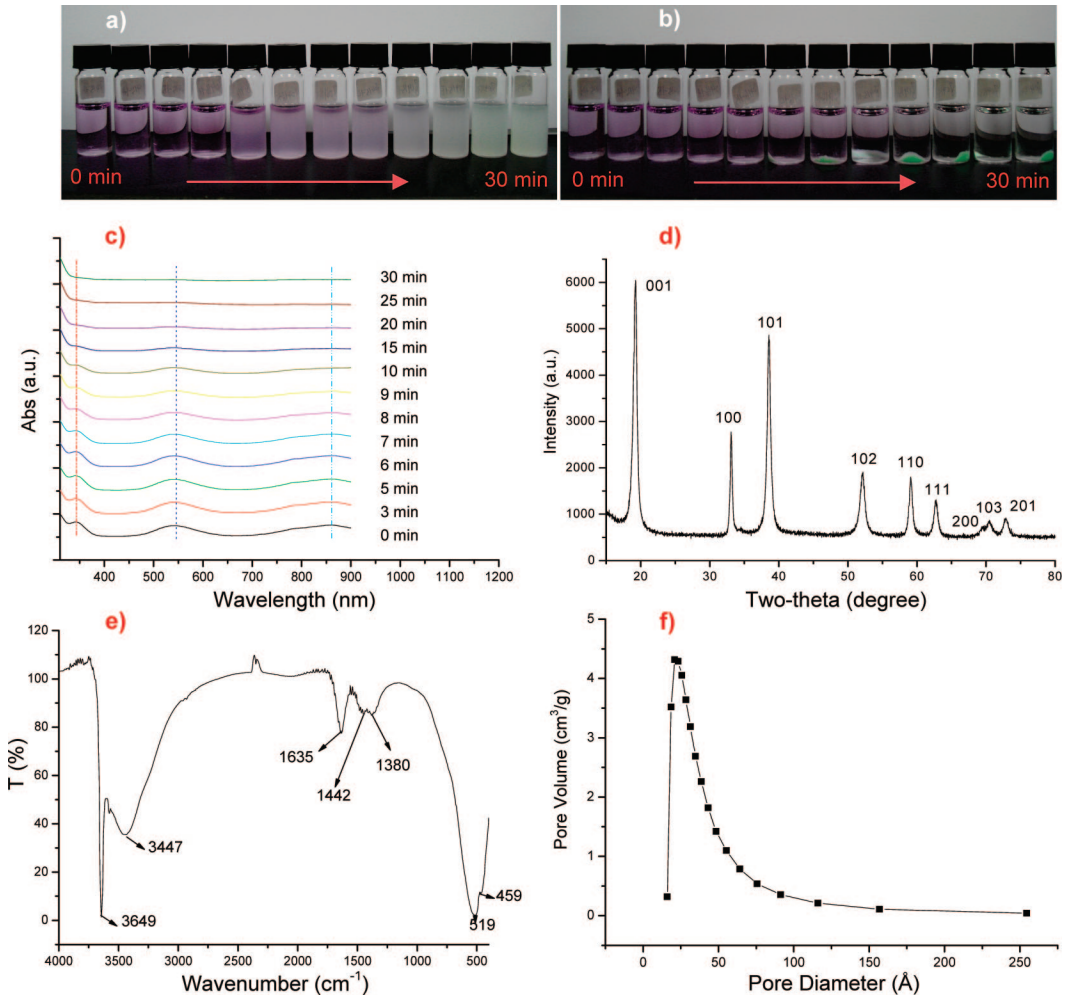

Figure 2. Photographs of the as-prepared samples after different reaction times at 100 °C: (a) before centrifuging and (b) after centrifuging; UV−vis spectra of the corresponding solution phases are displayed in (c). Materials characterization for the as-prepared hollow spheres of β-Ni(OH)$_2$ (refer to Figure 3): (d) XRD pattern, (e) FTIR spectrum, and (f) pore size distribution.

In addition to the above methods, in the present study, we develop a novel template-free approach for construction of β-Ni(OH)$_2$ hollow spheres. This wet chemical process allows one to directly prepare this metal hydroxide into size-controllable hollow spheres with the nanobuilding units (i.e., flakes and platelets). More importantly, on the basis of this self-assembled hollow precursor, we have also developed synthetic methods for preparations of 10 different nanostructured derivatives such as phase-pure metal and metal oxide nanostructures Ni and NiO, metal and metal oxide nanocomposite NiO/Ni, metal and metal hydroxide nanocomposite Ni/β-Ni(OH)$_2$, metal/metal oxide and carbon nanotube (CNT) nanocomposites CNT/NiO, CNT/Ni, and Ni@CNTs, and metal hydroxide and metal hydroxide nanocomposites Mg(OH)$_2$/β-Ni(OH)$_2$, Co(OH)$_2$/β-Ni(OH)$_2$, and Fe(OH)$_3$/β-Ni(OH)$_2$. This research endeavor is significant because we feel that most of nanomaterials and their syntheses at the present time have been investigated and reported separately as individual cases, and interconnection or interrelation among their various derivatives in synthesis is somehow lacking. To this end, our efforts herein would serve as the first attempt of this type of systematic investigation for nickel-related nanomaterials, and thus a greater picture for the chemical conversions (in liquid phase, solid state, and solid−gas reactions) of this materials family has been obtained, as summarized in Figure 1.

2. Experimental Section

2.1. Preparation of Hollow Spheres of β-Ni(OH)$_2$. First, as a starting structural basis for a variety of other nanostructures and nanocomposites prepared in this work, self-assembled hollow spheres of β-Ni(OH)$_2$ were synthesized. Briefly, varied amounts of 1,2-ethanediamine ($C_2H_4(NH_2)_2$, EDA; 0.0005−0.25 mL; 99 wt

(50) Xu, L. P.; Ding, Y.-S.; Chen, C.-H.; Zhao, L. L.; Rimkus, C.; Joesten, R.; Suib, S. L. *Chem. Mater.* **2008**, *20*, 308–316.
(51) Shan, Z. W.; Stach, E. A.; Wiezorek, J. M. K.; Knapp, J. A.; Follstaedt, D. M.; Mao, S. X. *Science* **2004**, *305*, 654–657.
(52) Park, J.; Kang, E.; Son, S. U.; Park, H. M.; Lee, M. K.; Kim, J.; Kim, K. W.; Noh, H.-J.; Park, J.-H.; Bae, C. J.; Park, J.-G.; Heyon, T. *Adv. Mater.* **2005**, *17*, 429–434.
(53) Leng, Y. H.; Li, Y.; Li, X. G.; Takahashi, S. *J. Phys. Chem. C* **2007**, *111*, 6630–6633.
(54) Han, M.; Liu, Q.; He, J. H.; Song, Y.; Xu, Z.; Zhu, J. M. *Adv. Mater.* **2007**, *19*, 1096–1100.
(55) Jia, F. L.; Zhang, L. Z.; Shang, X. Y.; Yang, Y. *Adv. Mater.* **2008**, *20*, 1050–1054.
(56) Winnischofer, H.; Rocha, T. C. R.; Nunes, W. C.; Socolovsky, L. M.; Knobel, M.; Zanchet, D. *ACS Nano* **2008**, *2*, 1313–1319.
(57) Wu, Z. Y.; Liu, C. M.; Guo, L.; Hu, R.; Abbas, M. I.; Hu, T. D.; Xu, H. B. *J. Phys. Chem. B* **2005**, *109*, 2512–2515.
(58) Needham, S. A.; Wang, G. X.; Liu, H. K. *J. Power Sources* **2006**, *159*, 254–257.
(59) Parada, C.; Morán, E. *Chem. Mater.* **2006**, *18*, 2719–2725.

%) and nickel-nitrate aqueous solution [$Ni(NO_3)_2 \cdot 6H_2O$; 0.0025−0.25 mL; 0.50 M] were sequentially added to a glass bottle (capacity of 4 mL) which contained 2.4−2.5 mL of NaOH aqueous solution (0−10.0 M), followed by a thorough mixing of all reagents. In actual synthetic preparations, for example, 0.4 mL of 0.5 M $Ni(NO_3)_2 \cdot 6H_2O$ and 80 μL of EDA (99 wt %) were mixed thoroughly, which was then divided as four equal portions and added into four glass bottles (volume capacity = 4 mL; each bottle contained 2.4 mL of 7 M NaOH solution), respectively. Afterward, the bottles were placed in an electric oven set at 100 °C for 0−3 h (mostly for 30 min); light green β-$Ni(OH)_2$ solid products were harvested with centrifugation−redispersion cycles using deionized water three times and then dried at 60 °C overnight.

2.2. Preparation of Hollow NiO Nanostructures. Hollow NiO nanostructures were prepared by thermal decomposition of the above as-synthesized β-$Ni(OH)_2$ at 400 °C for 2 h in laboratory air in a tubular electric furnace (Figure 1).

2.3. Preparation of Hollow Ni Nanostructures and NiO/Ni Nanocomposites. Hollow Ni nanostructures were prepared by heating the above as-synthesized β-$Ni(OH)_2$ (specified in Subsection 2.1) in a H_2 gas flow (10−35 mL/min) at 450 °C for 1 h in a horizontal quartz-tube reactor (Figure 1). Reaction products were still kept in the same H_2 gas stream after the power of the furnace was shut down. Furthermore, reoxidation of certain as-prepared Ni nanostructures (e.g., prepared with a H_2 gas flow of 10 mL/min) in laboratory air led to self-ignition and thus formation of NiO/Ni nanocomposites (Figure 1).

2.4. Preparation of Hollow Ni/β-$Ni(OH)_2$ Nanocomposites. Ni/β-$Ni(OH)_2$ nanocomposites were obtained by using hydrazine to partially deoxidize the β-$Ni(OH)_2$ solid precursor. In a typical synthesis, 0.1 mL of hydrazine (35 wt %) and 2.5 mL of NaOH (7.0 M) aqueous solution were sequentially added to a glass bottle (capacity 4 mL) containing the above prepared β-$Ni(OH)_2$ (Subsection 2.1), followed by a thorough mixing of all reagents. The bottle was then placed in an electric oven set at temperatures over 60−100 °C for 0.5−3 h (Figure 1). Reaction products were harvested with centrifugation−redispersion cycles using deionized water three times.

2.5. Preparation of CNTs/Ni Nanocomposites. Two chemical vapor deposition (CVD) methods were developed for preparation of CNTs/Ni nanocomposites. (i) One-step method (Figure 1): Experiments were carried out in a horizontal quartz-tube reactor (inner diameter of 7 mm) with acetylene C_2H_2 diluted with purified argon gas. The above prepared hollow spheres of β-$Ni(OH)_2$ (i.e., the precursor of catalyst; Subsection 2.1) were supported on glass wool and pressed into a small packed catalyst bed. The β-$Ni(OH)_2$ powder was heated in an electric furnace inside an acetylene/argon gas mixture. In most cases, the argon was fed as a background gas at a constant feed rate of 75 mL/min, and the carbon source gas acetylene was introduced at a variable rate of 5−10 mL/min when the temperature reached a desired value (mostly set at 450 °C). This CVD process was kept running for 5−20 min, and then the C_2H_2 stream was turned off. The reaction product was retained in the argon stream for 1 h after the power of the furnace was shut down. The black powder product was then collected and stored in a clean glass bottle for further materials characterization. (ii) Two-step method (Figure 1): In the first step, metallic nanoflowers of Ni (catalysts) were prepared by deoxidizing β-$Ni(OH)_2$ at 450 °C in a H_2 stream at flow rate of 10 mL/min for 20 min. In the second step, a gas flow of acetylene and argon was introduced (as detailed in Method (i), herein the flow rate of C_2H_2 = 5 mL/min, and the flow rate of Ar = 75 mL/min) at 450 °C for 5 min, followed by the same cooling and collecting procedures.

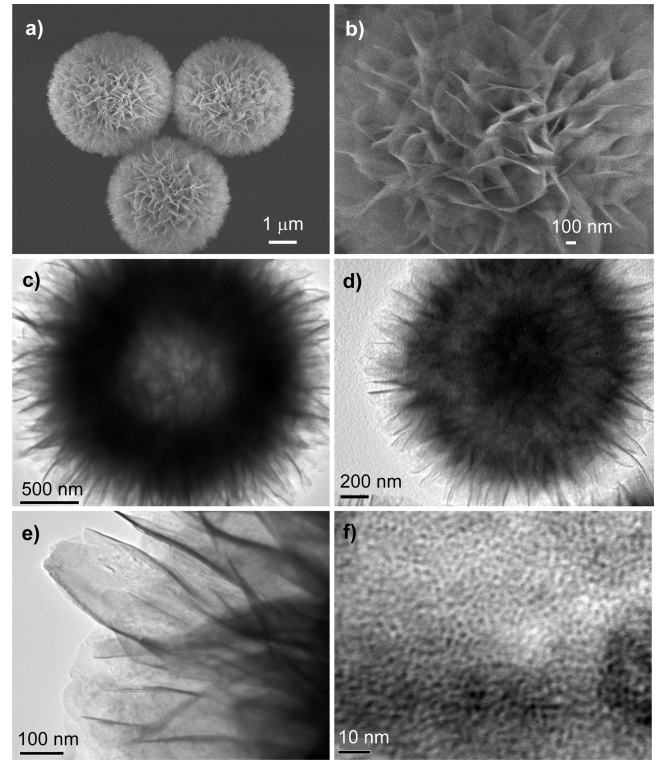

Figure 3. FESEM images (a, b) and TEM images (c−f) of the as-prepared hollow spheres of β-$Ni(OH)_2$ at different magnifications. Image (f) shows detailed structures of β-$Ni(OH)_2$ "petals" (image e).

2.6. Preparation of CNTs/NiO Nanocomposites. As described in Figure 1, CNTs/NiO nanocomposites were prepared in a horizontal quartz-tube reactor (inner diameter of 7 mm) with acetylene C_2H_2 diluted with purified argon gas (also see Subsection 2.5). The above prepared hollow NiO nanostructures (i.e., catalysts, Subsection 2.2) were supported on glass wool and pressed into a small packed catalyst bed. The NiO powder was heated in an electric furnace to 400−500 at 10 °C/min and purged with an argon stream, in which the argon was fed as a background gas at a constant feed rate of 75 mL/min and the carbon source gas acetylene was introduced at a variable rate of 5−10 mL/min when the temperature reached a desired value (mostly at 400−450 °C). This CVD process lasted 3−20 min and after which the C_2H_2 stream was turned off while the product was still kept inside the argon stream for 1 h. The black powder product was then collected and stored in a clean glass bottle for later materials characterization.

2.7. Preparation of $Mg(OH)_2$/β-$Ni(OH)_2$ Nanocomposites. $Mg(OH)_2$/β-$Ni(OH)_2$ nanocomposites were prepared using $Mg(NO_3)_2$ to react with NaOH in the presence of β-$Ni(OH)_2$ precursor (Figure 1). In a typical synthesis, 2.5 mL of deionized water, 0.5−1.0 mL of 0.05 M $Mg(NO_3)_2$ aqueous solution, and 1.0−2.0 mL of 0.05 M NaOH aqueous solution were sequentially added to a glass bottle (capacity 4 mL) containing the above prepared hollow β-$Ni(OH)_2$ spheres (Subsection 2.1) under magnetic stirring at room temperature for 1 h. Products were harvested with centrifugation−redispersion cycles using deionized water three times. A light green powder was then obtained.

2.8. Preparation of $Co(OH)_2$/β-$Ni(OH)_2$ Nanocomposites. $Co(OH)_2$/β-$Ni(OH)_2$ nanocomposites were prepared using $Co(NO_3)_2$ to react with NaOH in the presence of β-$Ni(OH)_2$ precursor (Figure 1). In this synthesis, 2.5 mL of deionzed water, 0.5 mL of 0.05 M $Co(NO_3)_2$ aqueous solution, and 1.0 mL of 0.05 M NaOH aqueous solution were sequentially added to a glass bottle (capacity 4 mL) that contained the above prepared hollow β-$Ni(OH)_2$ spheres (Subsection 2.1) under magnetic stirring at room temperature for

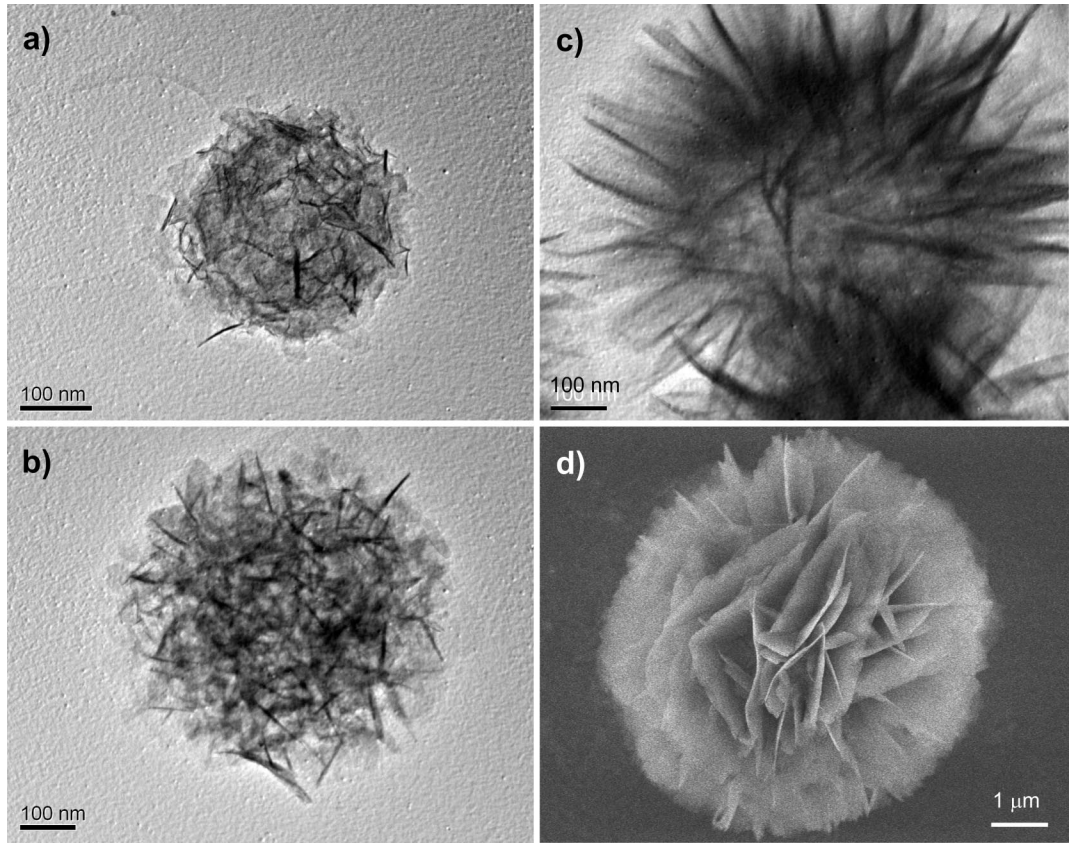

Figure 4. Size-controlled growth of β-$Ni(OH)_2$ spheres with different concentrations of $Ni(NO_3)_2$ in precursor solutions: (a) 0.5 mM (TEM image), (b) 1.0 mM (TEM image), (c) 5 mM (TEM image), and (d) 50 mM (FESEM image). Common experimental conditions: molar ratio $Ni^{2+}/C_2H_4(NH_2)_2 = 1/6$ and reaction time = 30 min.

1 h. Products were obtained after centrifugation−redispersion cycles using DI water three times. A light blue-green powder was then collected.

2.9. Preparation of $Fe(OH)_3$/β-$Ni(OH)_2$ Nanocomposites. $Fe(OH)_3$/β-$Ni(OH)_2$ nanocomposites were prepared using $Fe(NO_3)_3$ to react with NaOH in the presence of the β-$Ni(OH)_2$ solid precursor (Figure 1). In the synthesis, 2.5 mL of deionized water, 1.0 mL of 0.05 M NaOH aqueous solution, and 0.3 mL of 0.05 M $Fe(NO_3)_3$ aqueous solution and were sequentially added to a glass bottle (capacity 4 mL) containing the above prepared hollow β-$Ni(OH)_2$ spheres (Subsection 2.1) under magnetic stirring at room temperature for 1 h. Products were harvested with centrifugation−redispersion cycles using deionized water three times. A brown powder was then obtained.

2.10. Materials Characterization. UV−vis spectroscopy of the reaction solutions at different times was used to investigate the reaction process, recorded on a UV−vis spectrophotometer (Shimadzu UV-2450), using an aqueous solution of 7 M NaOH as reference. Identical starting solutions (i.e., specified the example of Subsection 2.1) were injected into 12 glass bottles and were then placed in an electric oven with temperature at 100 °C for 0, 3, 5, 6, 7, 8, 9, 10, 15, 20, 25, and 30 min, respectively. Afterward, the glass bottles were centrifugated at 6000 rpm for 5 min, and the separated clear solutions were used to perform UV−vis analysis at room temperature. The crystallographic phases of all as-prepared samples were investigated using the powder X-ray diffraction method (XRD, Shimadzu XRD-6000, Cu Kα radiation, $\lambda = 1.5406$ Å) at a scanning rate of 2°/min. The dimension, morphology, structure, and chemical composition of the samples were examined using field emission scanning electron microscopy and energy dispersive X-ray spectroscopy (FESEM/EDX; JSM-6700F), transmission electron microscopy and small area electron diffraction (TEM/EDX/SAED; JEM 2010, 200 kV), and high resolution transmission electron microscopy (HRTEM/EDX/SAED; JEM 2100F, 200 kV). Thermogravimetric analysis (TGA/DTG; Shimadzu TGA-50) measurements were carried out at a heating rate of 10 °C/min in purified air atmosphere. Specific surface area measurement and porosity analysis for the as-prepared β-$Ni(OH)_2$ (Subsection 2.1) and NiO (Subsection 2.2) samples were performed using N_2 adsorption−desorption isotherms (Quantachrome NOVA-3000 system at 77 K). Prior to measurements, the samples were degassed at 100 °C overnight.

3. Results and Discussion

Figure 1 shows a schematic description of hollow spheres of β-$Ni(OH)_2$ and related chemical conversions to many different nano-derivatives investigated in this work. Starting with the nickel nitrate and ethylenediamine, flower-like hollow spheres of β-$Ni(OH)_2$ can be prepared in basic solutions. In Figure 2a,b, the sample bottles show a sequential color change from rosy purple starting precursor solution to light green β-$Ni(OH)_2$ product with increase in reaction time. UV−vis absorption spectra measured for the reaction solution phases are also displayed in Figure 2c. As described in eq 1, the major Ni^{II} complex species present in the starting solutions is 6-coordinated $[Ni(EDA)_3]^{2+}$ (where EDA = 1,2-ethanediamine) under our preparative conditions. In particular, three observed bands at 345, 542, and 880 nm can be readily assigned to $^3A_{2g} \rightarrow {}^3T_{1g}(P)$, $^3A_{2g} \rightarrow {}^3T_{1g}(F)$, and $^3A_{2g} \rightarrow {}^3T_{2g}$ of the octahedral complex $[Ni(EDA)_3]^{2+}$ on the basis

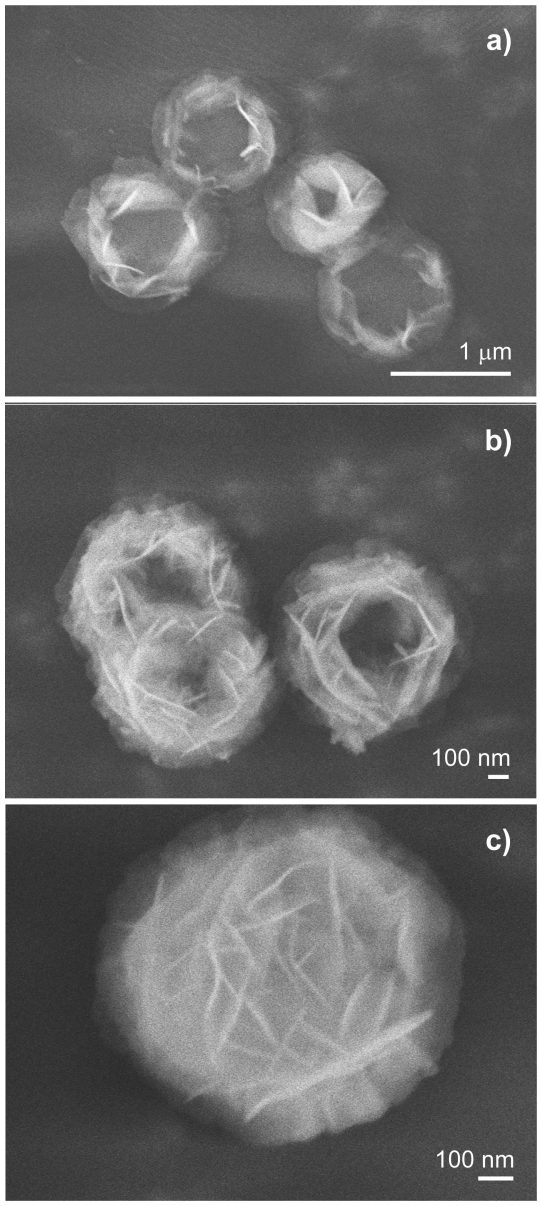

Figure 5. Donut-like intermediate of β-$Ni(OH)_2$ petal assemblies (a, b, FESEM images), which forms the basic structure for final hollow spheres of β-$Ni(OH)_2$ (c, FESEM image). Experimental conditions: molar ratio $Ni^{2+}/C_2H_4(NH_2)_2$ = 1/10 and reaction time = 15 min.

of a D_3 symmetry.[63,64] The above characteristic absorptions can be used to monitor the reaction extent of β-$Ni(OH)_2$ formation. After 30 min of reaction, for example, all the three bands disappear, indicating that there is no more $[Ni(EDA)_3]^{2+}$ in the solution phase, and the formation reaction of β-$Ni(OH)_2$ is complete; this chemical stoichiometry is shown in eq 2. The function of EDA used herein is to lower the precipitation rate of β-$Ni(OH)_2$ and thus to enhance the product regularity.

(60) Zhu, J. X.; Gui, Z.; Ding, Y. Y.; Wang, Z. Z.; Hu, Y.; Zou, M. Q. *J. Phys. Chem. C* **2007**, *111*, 5622–5627.
(61) Varghese, B.; Reddy, M. V.; Zhu, Y. W.; Chang, S. L.; Teo, C. H.; Subba Rao, G. V.; Chowdari, B. V. R.; Wee, A. T. S.; Lim, C. T.; Sow, C.-H. *Chem. Mater.* **2008**, *20*, 3360–3367.
(62) Li, Y. G.; Tan, B.; Wu, Y. Y. *Chem. Mater.* **2008**, *20*, 567–576.
(63) Cotton, F. A.; Wilkinson, G. *Advanced Inorganic Chemistry*, 4th ed.; John Willey & Sons: New York, 1980; Chapter 21, p 787.
(64) Négrier, F.; Marceau, E.; Che, M.; Giraudon, J.-M.; Gengembre, L.; Löfberg, A. *J. Phys. Chem. B* **2005**, *109*, 2836–2845.

$$Ni^{2+}(aq) + 3EDA(aq) \rightarrow [Ni(EDA)_3]^{2+}(aq) \quad (1)$$

$$[Ni(EDA)_3]^{2+}(aq) + 2OH^-(aq) \rightarrow \beta\text{-}Ni(OH)_2(s) + 3EDA(aq) \quad (2)$$

The light green products (β-$Ni(OH)_2$) are examined with microscopic methods. Figure 3 shows some representative images of their morphologies. The prepared β-$Ni(OH)_2$ products are actually microspheres that comprise solid flakes. The individual flakes are curved and connected to each other (Figure 3a,b; also will be characterized shortly in Figure 4). More intriguingly, these dandelion-like β-$Ni(OH)_2$ spheres have interior space(s). As shown in Figure 3, two types of interior structures are found: (i) single-shelled spheres (Figure 3c) and (ii) core−shell spheres (Figure 3d). In the latter case, an additional void in the central core is often found (i.e., double-shelled structure). On the basis of our TEM image statistics, the population ratio between the type (i) and the type (ii) spheres is estimated at 3:1 under our typical synthetic conditions (Subsection 2.1). It should be mentioned that while synthesis of nanostructured β-$Ni(OH)_2$ spheres had been studied extensively,[41−50] our template-free synthesis of hollow β-$Ni(OH)_2$ spheres with complex interior structures is a novel self-assembly approach. The petal-like flakes of β-$Ni(OH)_2$ on the shell structures are standing along the radial directions of spheres while they seem to be quite flexible (Figure 3b,e), reflecting their ultrathin feature. A more detailed view on the β-$Ni(OH)_2$ "petals" is displayed in Figure 3f. The self-assembled β-$Ni(OH)_2$ petals consist of even smaller nanocrystallites at the sizes of 3−4 nm. However, metal hydroxides are also prone to high energy electrons (i.e., under TEM electron beam irradiation). Therefore, apart from the β-$Ni(OH)_2$ nanocrystallites in Figure 3f, formation of partially dehydrated products (e.g., NiO nanocrystallites together with β-$Ni(OH)_2$ main phase) cannot be entirely ruled out using the TEM data alone; this point will be further addressed together with our BET/BJH investigation results (Figure 2f).

β-$Ni(OH)_2$ is isomorphous with brucite $Mg(OH)_2$.[41] The crystallographic structure of hollow spheres of β-$Ni(OH)_2$ has been investigated with XRD in this work; all diffraction peaks in Figure 2d can be indexed perfectly to a brucite-like hexagonal crystal phase (space group: $P\bar{3}m1$; a_o = 3.126 Å, and c_o = 4.605 Å; JCPDS file no. 14-0117);[41−50] no peaks from the α-$Ni(OH)_2$ phase were observed.[41] In particular, the 001 diffraction is more intense than the 100, indicating the {001} surfaces are indeed predominant in the phase pure β-$Ni(OH)_2$ flakes. The FTIR spectrum shown in Figure 2e reveals chemical information and major functional groups in the β-$Ni(OH)_2$. The sharp peak at 3649 cm^{-1} is assigned to the stretching vibrational mode (ν_{OH}) of non-hydrogen-bonded hydroxyl groups in the brucite-like sheets, while the broadband at 3447 cm^{-1} to the stretching mode of hydrogen-bound hydroxyl groups in the same layered structure. The latter band (i.e., 3447 cm^{-1}) and a strong absorption at 1635 cm^{-1} can also be ascribed to the stretching and bending modes of surface-adsorbed/trapped (hydrogen-bonded) water molecules.[41] The peak at 519 cm^{-1} is attributed to the in-plane deformation vibration of water (δ_{OH}) and the shoulder absorption at 459 cm^{-1} to the stretching vibration of Ni−OH ($\nu_{Ni\text{-}OH}$).[41] The large water peaks observed are consistent with

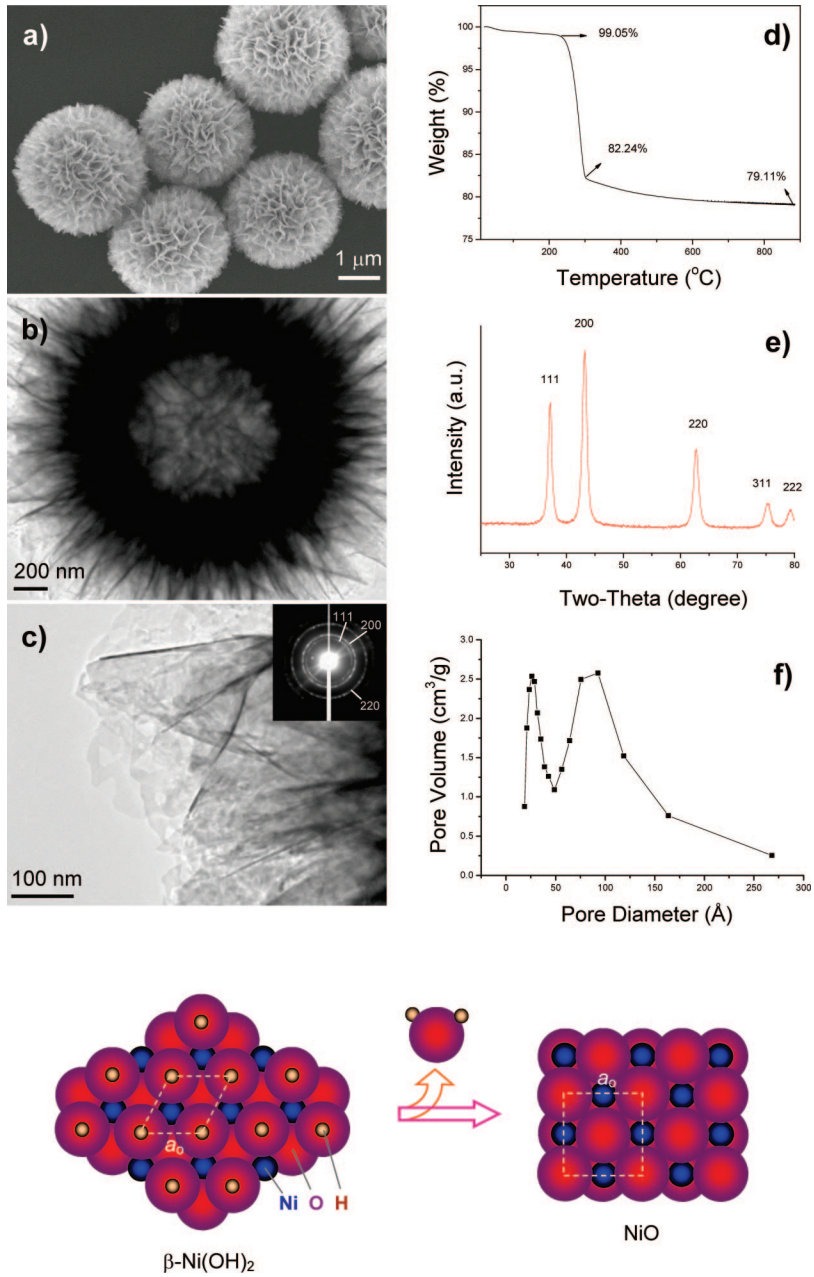

Figure 6. (a−c) Hollow spheres of NiO formed from thermal decomposition of hollow spheres of β-Ni(OH)$_2$ (a, FESEM image; b and c, TEM images; and the inset in c is a SAED pattern), (d) TGA scan of hollow spheres of β-Ni(OH)$_2$, (e) XRD pattern of resultant hollow spheres of NiO, and (f) pore-size distribution of NiO hollow spheres. Color inset illustrates a proposed mechanism for thermal decomposition of β-Ni(OH)$_2$ to NiO, in which the (001) plane of β-Ni(OH)$_2$ and the (100) plane of NiO are shown; a_o are lattice constants of the respective unit cells (marked with dashed frames).

the common features of β-Ni(OH)$_2$, and it is easy to include intersheet water. As a result of the basicity of metal hydroxides, it is not surprising to see the adsorption of atmospheric carbon dioxide and therefore the presence of carbonate anions on the surfaces of the β-Ni(OH)$_2$ spheres, as shown in the small peaks at around the 1442 cm^{-1} range for this anion.[13,14] The peak at approximately 1380 cm^{-1} is attributable to a trace surface adsorption of nitrate ions (ν_3 vibration mode of NO_3^-; this anion was from the starting nickel nitrate).[13,14] No organic vibrations (e.g., C−C and C−H) were observed in their respective fingerprint regions, which reveals that the chelating agent 1,2-ethanediamine was not incorporated in the hollow spheres. As expected for the observed porous nature, our typical β-Ni(OH)$_2$ spheres have a large specific surface area of 93.2 m^2/g, with a unimodal pore-size distribution located across the range of 2−5 nm (reported in Figure 2f). Quite interestingly, the measured mesoporosity by the Barrett−Joyner−Halenda method is also consistent with our direct TEM observation on the intercrystallite spaces (e.g., Figure 3f).[65] Therefore, the small crystallites (3−4 nm; Figure 3f) in the β-Ni(OH)$_2$ flakes do not result from the electron beam irradiation; they are pristine nanocrystallites. In agreement with this, lattice fringes of d_{100} can be viewed in our HRTEM study in which the incident electron beam was pointed perpendicularly to the surfaces

(65) Sing, K. S. W.; Everett, D. H.; Haul, R. A. W.; Moscou, L.; Pierotti, R. A.; Rouquerol, J.; Siemieniewska, T. *Pure Appl. Chem.* **1985**, *57*, 603–619.

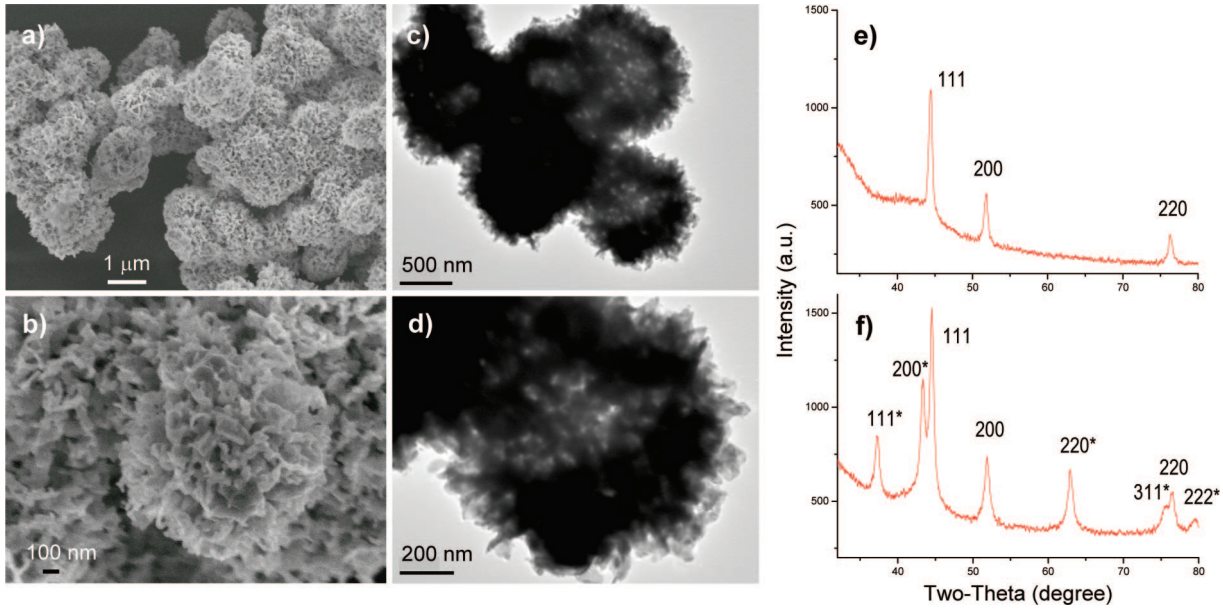

Figure 7. (a−d) Porous metallic Ni formed from thermal reduction of hollow spheres of β-Ni(OH)$_2$ (a and b, FESEM images; c and d, TEM images), (e) XRD pattern of resultant porous metallic Ni product, and (f) XRD pattern of NiO/Ni nanocomposite resulted from self-ignition in air; diffraction peaks of NiO phase are indicated with an asterisk. H_2 flow rates used in the reduction reactions: (a−e) 35 mL/min and (f) 10 mL/min.

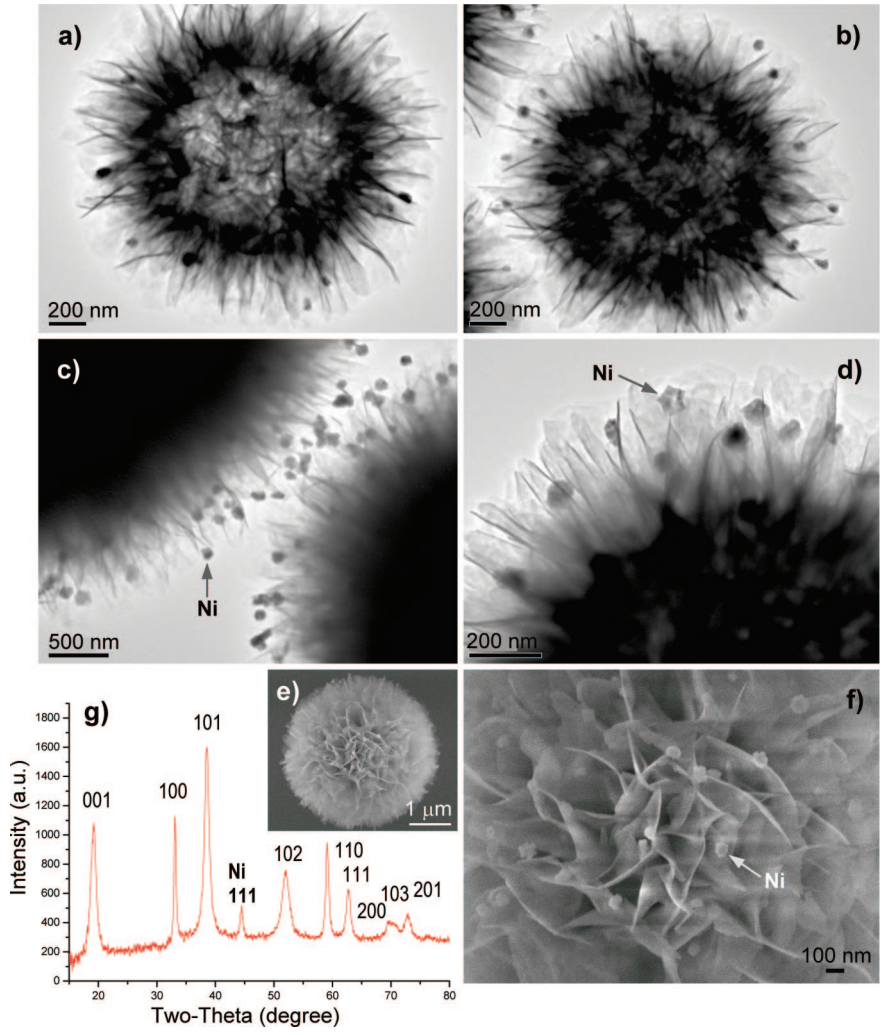

Figure 8. (a−f) Morphologies of Ni/β-Ni(OH)$_2$ nanocomposites [a−d, TEM images; e and f (the central part of image e), FESEM images] and (g) XRD pattern of Ni/β-Ni(OH)$_2$ nanocomposite, noting that the 111 diffraction of metallic Ni can be clearly seen.

of the {001}. Further details can be obtained from Supporting Information (SI-1).

Various process parameters have been optimized in this work (Subsection 2.1). Among them, the concentration of

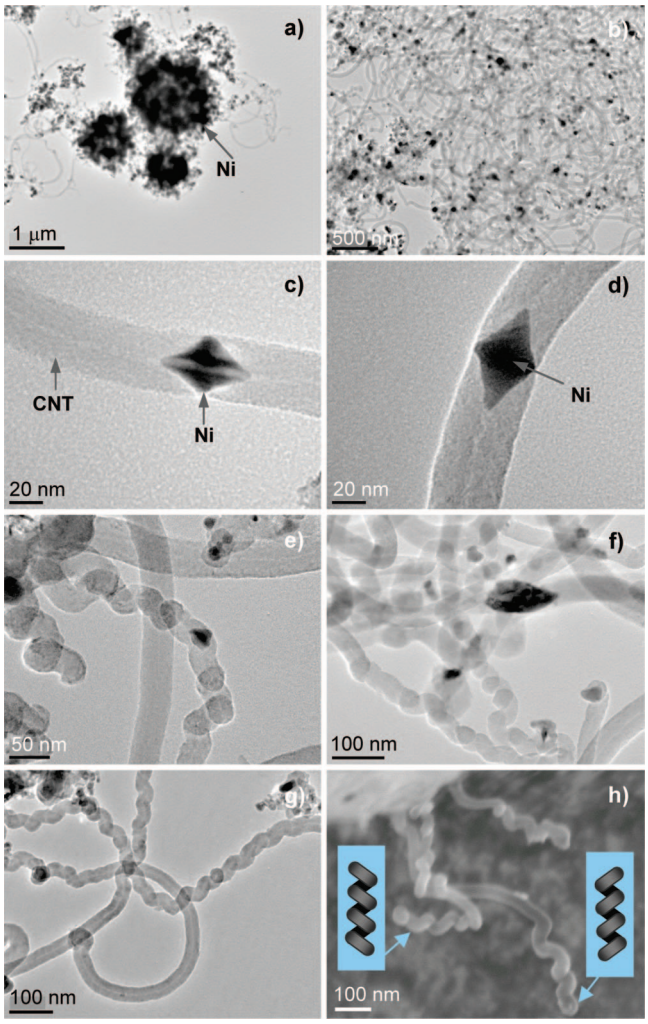

Figure 9. CNTs/Ni nanocomposite (a, TEM image) and Ni@CNTs nanocomposites (b−d, TEM images), spiral CNTs (e−g, TEM images), and helical CNTs formed on the surface of Ni spheres (h, FESEM image). These samples were formed from hollow spheres of β-Ni(OH)$_2$ at 450 °C with a gas stream of C_2H_2 and Ar (Method (i), Subsection 2.5; refer to Figure 1).

divalent nickel in the starting solutions plays the most important role in controlling the size of resultant spheres. In Figure 4, four representative β-Ni(OH)$_2$ spheres are displayed. It is clearly demonstrated that the size-controlled growth can be manipulated well with starting concentrations of Ni^{2+} and EDA. Furthermore, the thickness of the β-Ni(OH)$_2$ flakes, which is shown as thin lines in the microscopic images, can also be controlled in the range of 5 nm (image a) to 20 nm (image c) or a few tens of nanometers (image d) with an increase in starting concentrations. However, when the Ni^{2+} concentration is lower than 5 mM (Figure 4a,b), only solid β-Ni(OH)$_2$ spheres can be obtained. This is because thin and soft β-Ni(OH)$_2$ flakes aggregate more easily into a compact form. When the Ni^{2+} concentration is equal to or high than 5 mM (Figure 4c,d), hollow spheres of β-Ni(OH)$_2$ can then be prepared. To understand the formation of hollow interiors, we have also carried out a mechanistic investigation. By introducing more EDA to synthesis (e.g., Ni^{2+}/EDA = 1/10), we were able to lower the speed of β-Ni(OH)$_2$ precipitation and arrest solid intermediates. Surprisingly, in such intermediates, the β-Ni(OH)$_2$ flakes self-assembled into a donut-like ring structure. Some of these donut-rings are shown in Figure 5a,b, noting that they are eventually turned into complete hollow spheres when more β-Ni(OH)$_2$ flakes are added to the ring structure (Figure 5c). The self-assembly mechanism revealed herein for the formation of a hollow interior is different from a reported one,[45] in which a solid hollowing process of 24 h with Ostwald ripening was required under hydrothermal conditions (at 100−180 °C).[30,38,40]

With the above-prepared hollow spheres of β-Ni(OH)$_2$, we have investigated formations of various Ni-containing nanoderivatives, as detailed in the flowchart of Figure 1. As the first example, hollow spheres of NiO can be obtained from thermal decomposition of hollow spheres of β-Ni(OH)$_2$, as indicated in eq 3. As reported in Figure 6a, hollow spheres of NiO retain the similar product morphology and size to those in Figure 2. In this connection, importantly, the interior spaces of the hollow spheres are well preserved upon the thermal treatment (400 °C, Figure 6b; see Experimental Section) in laboratory air. To understand this conversion process, we also conducted a thermogravimetric analysis in an air stream. In Figure 6d, it is found that while trapped moisture (about 1%) can be removed in the early stage of this process (up to 200 °C), the thermal decomposition of β-Ni(OH)$_2$ is largely completed at 300 °C. The weight loss over 300 to 800 °C can be assigned to a continuous thermal depletion of deep-trapped hydroxyl groups and removal of chemisorbed carbonate anions. The theoretical weight loss for the decomposition reaction (eq 3) is 19.4%. Our experimental value here (99.05%−79.11% = 19.9%) is in good agreement with the theoretical data. The slight increase in the value is due to the loss of surface-adsorbed species, as discussed above and revealed in our FTIR investigation (Figure 2e). The resultant hollow spheres of NiO are well crystallized, which is reflected in sharp diffraction rings of the SAED pattern and well-defined phase-pure XRD patterns of Figure 6c,e (space group: $Fm\bar{3}m$; a_o = 4.178 Å; JCPDS file no. 71-1179).[57−62] The phase transformation of β-Ni(OH)$_2$ to NiO causes a crystallographic structural change from the hexagonal system to the cubic system. Because the intensity of the 200 diffraction peak is clearly higher than those of others, it can be deduced that the boundary faces of the NiO flakes (Figure 6c) are mainly the {100} surfaces of this rock salt structure. The formation of these nonpolar crystal planes is understandable. Topotatically, transformation of the {001} faces of hexagonal β-Ni(OH)$_2$ to the {100} faces of rock-salt NiO involves the least structural change, since a simple removal of water molecules from hydroxyl groups between brucite-like sheets can easily realize this process, as depicted in Figure 6 (color inset). Through this conversion, the specific surface area of the resultant NiO spheres is about 114.2 m^2/g; this value is larger than that of their precursor β-Ni(OH)$_2$ spheres (93.2 m^2/g) and much larger than that obtained in nanocolumn porous NiO (42.3 m^2/g).[60] Quite interestingly, in Figure 6f, the pore size distribution shows a bimodal hierarchical structure. There are two types of pores in the pore-diameter profile, one peaked at 2−5 nm (similar to

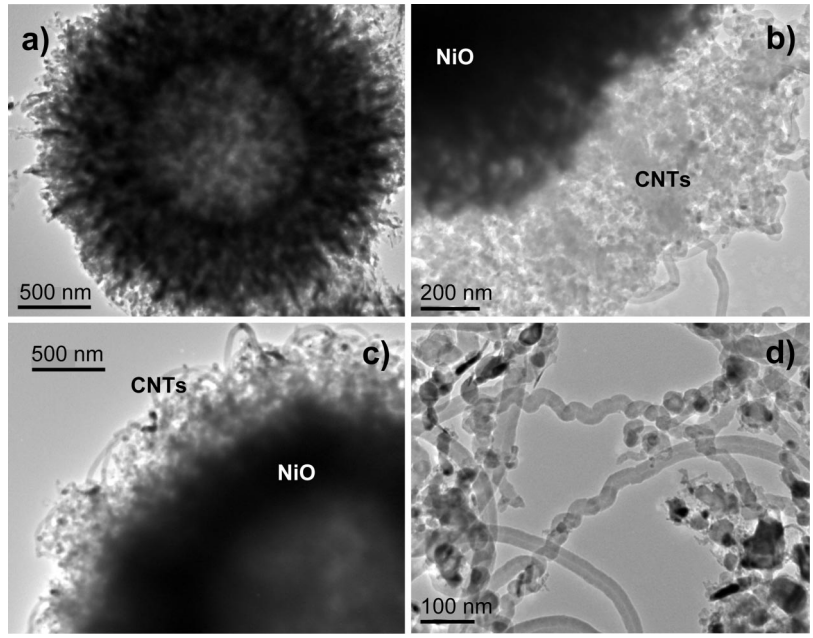

Figure 10. TEM images of hollow spheres of NiO after reaction with a mixed stream of C_2H_2 and Ar at 400 °C for 3 min (a) and of CNTs/NiO nanocomposites formed with the same mixture stream of C_2H_2 and Ar at 450 °C for 10 min (b and c) and for 20 min (d) which shows formation of helical CNTs. Experimental details can be found in Subsection 2.6 (refer to Figure 1).

Figure 2f) and the other at 5−15 nm. The formation of large mesopores can be considered as a result of shrinkage of brucite-like sheets of β-$Ni(OH)_2$ when they are condensed into the NiO phase (Figure 6) with release of water, noting a considerable difference in the densities between β-$Ni(OH)_2$ and NiO (4.15 g/cm^3 vs 6.67 g/cm^3). Similar to their mesocrystalline precursor β-$Ni(OH)_2$, crystallographic orientations among the NiO crystallites are still kept in the petal-like NiO flakes after thermal decomposition, as revealed in our HRTEM investigation that shows large areas of crystalline NiO across the petal textures (Supporting Information, SI-2).

$$\beta\text{-Ni(OH)}_2(s) \rightarrow \text{NiO}(s) + \text{H}_2\text{O}(g) \qquad (3)$$

In addition to the above thermal conversion, the hollow spheres of β-$Ni(OH)_2$ can also be turned into porous metallic nickel with reducing agents, such as shown in eq 4 with hydrogen. In Figure 7, we present the product morphologies of porous nickel formed after a reduction in hydrogen atmosphere at 450 °C (Figure 1). Although the shape of individual spheres is still recognizable, the resultant nickel spheres are fused together during the reduction reactions (Figure 7a,b). Nevertheless, in addition to their porous appearance, they still preserve their initial hollow interiors, since the central cavity of individual hollow spheres can be virtualized clearly in our TEM images (Figure 7c,d). The XRD pattern in Figure 7e indicates the porous nickel has an fcc crystal structure (space group: $Fm\bar{3}m$; a_o = 3.45 Å; JCPDS file no. 88-2326).[51−56] In some cases, interestingly, the metallic products can self-ignite when handled in laboratory air and turn into oxidative forms. This surface oxidation is demonstrated with the XRD patterns of Figure 7f, in which the metallic nickel and nickel oxide phases are superimposed. Compared to alkali and earth alkali metals, which are much easier to burn in atmospheric ambience, the self-ignition of transition metals only takes places for the samples with fine crystallites and with very large surface areas. In the present cases, we find that when a higher flow rate of H_2 is used (Figure 7e), the resultant nickel crystallites are more stable in air and phase pure Ni can be obtained, whereas a slower flow rate of H_2 input would lead to formation of more active nickel which will burn in normal air and give rise to the fabrication of NiO/Ni binary composites (also refer to Figure 1). It can be thus deduced that the slower reaction rate favors formation of larger surface areas for metallic nickel. On the basis of the results of Figure 7e,f, we can further control chemical reactivity of the resultant nickel metals and thus design chemical compositions of reaction products by selecting the reaction rate in this type of synthesis.

$$\beta\text{-Ni(OH)}_2(s) + \text{H}_2(g) \rightarrow \text{Ni}(s) + 2\text{H}_2\text{O}(g) \qquad (4)$$

Instead of the above total reduction in gas phase, partial reduction of β-$Ni(OH)_2$ to metallic Ni can also be achieved in solution phase under moderate reducing conditions; this process leads to formation of Ni/β-$Ni(OH)_2$ binary composites, as illustrated in Figure 8. In the presence of N_2H_4, partial reduction of β-$Ni(OH)_2$ can take place at relatively low temperatures of 60−100 °C. In Figure 8a−f, the nickel nanoparticles are formed on the surface of hollow spheres of β-$Ni(OH)_2$. Because we do not observe separate free-standing nickel nanoparticles in our prepared samples, we believe that the petal-like flakes of β-$Ni(OH)_2$ also serve as starting nucleation points for the divalent nickel to metallic nickel conversion. As a result of to the limited reducing power of N_2H_4, the reduction mainly takes place on the external surfaces of β-$Ni(OH)_2$ spheres. For instance, the central cores of β-$Ni(OH)_2$ spheres seem to remain intact after the reduction reactions [Figure 8, part a (a hollow sphere) versus part b (a core−shell sphere)]. On the other

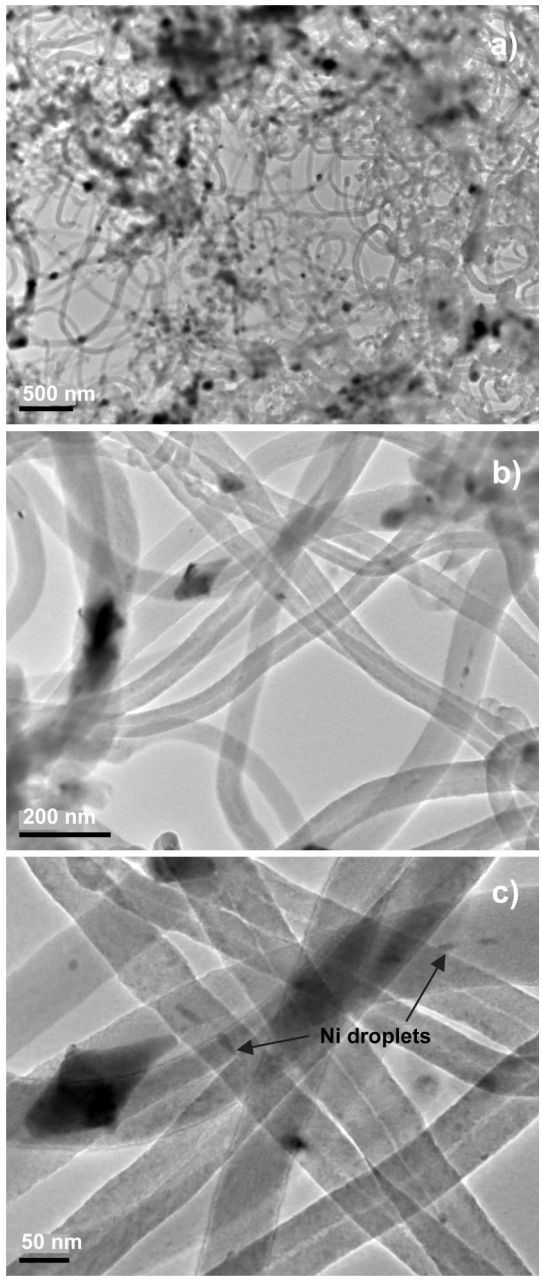

Figure 11. TEM images of CNTs/Ni nanocomposite (a) and Ni@CNTs nanocomposites (b,c). These samples were formed from porous metallic Ni at 450 °C with a gas stream of C_2H_2 and Ar (Method (ii), Subsection 2.5; refer to Figure 1).

hand, the size and population of surface nickel depend on the N_2H_4 concentration in the starting solutions and reaction temperature used in synthesis. The metallic nickel formed in this process also has an fcc crystal structure (space group: $Fm\bar{3}m$; a_o = 3.45 Å; JCPDS file no. 88-2326).[51−56] Both our XRD (Figure 8g) and HRTEM/SAED (Supporting Information, SI-3) investigations confirm this crystallographic phase for the metal nanoparticles.[51−56]

In view of their nanostructural natures, we further use the as-prepared β-Ni(OH)$_2$, NiO, and Ni spheres as catalytic materials to synthesize carbon nanotubes (CNTs), as schematically described in Figure 1. In these examples, the hollow spheres of β-Ni(OH)$_2$ can directly react with C_2H_2 at elevated temperatures, resulting in CNTs/Ni and Ni@CNTs types of

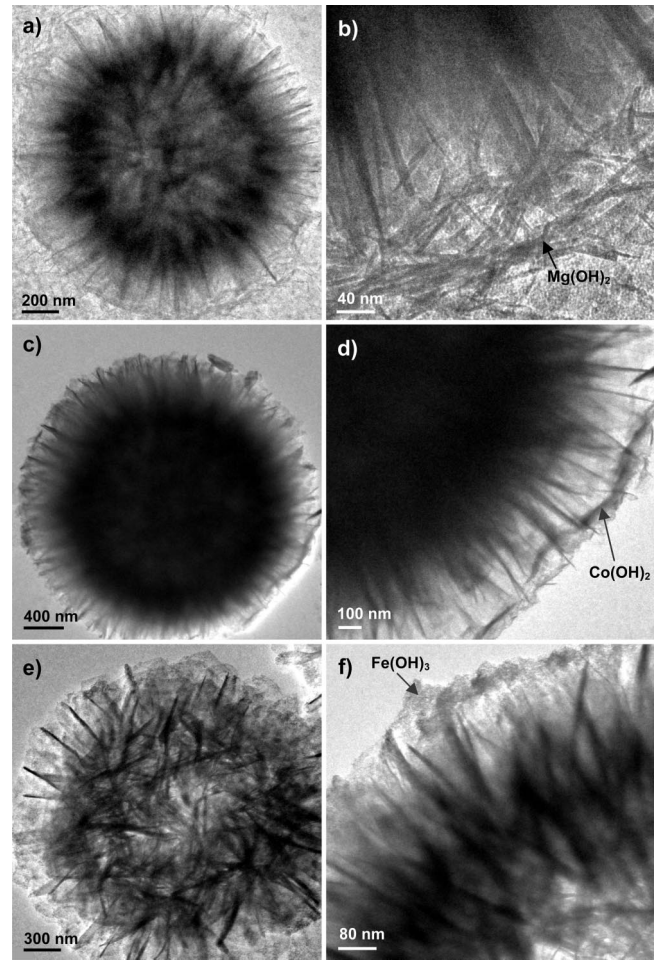

Figure 12. TEM images of Mg(OH)$_2$/β-Ni(OH)$_2$ nanocomposite (a and b), Co(OH)$_2$/β-Ni(OH)$_2$ nanocomposite (c and d), and Fe(OH)$_3$/β-Ni(OH)$_2$ nanocomposite (e and f). These samples were prepared with the precipitation of a surface phase to β-Ni(OH)$_2$ support at room temperature (refer to Figure 1).

nanocomposites. Chemically, the reduction of divalent nickel to metallic nickel is realized in the presence of C_2H_2 according to eqs 5 and 6. In Figure 9a, which shows the first type of nanocomposite (CNTs/Ni) formed from this process, the metallic nickel still keeps the spherical shape of precursor β-Ni(OH)$_2$ while the sphere surfaces are surrounded with CNTs. In Figure 9b, which gives an overall view of the second type of nanocomposite (Ni@CNTs), rhombic (or bicone shaped) nickel particles are included in individual CNTs, as detailed in Figure 9c,d. This type of M@CNTs (M = metal elements) has been observed with a number of transition metal catalysts (e.g., $Fe_{1-x}Cu_x$@CNTs, Co@CNTs, $Co_{1-x}Cu_x$@CNTs, $Co_{1-x}Ag_x$@CNTs, Ni@CNTs, and $Ni_{1-x}Cu_x$@CNTs) using other synthetic processes, where the CNTs are synthesized into the form of cone stacks or "herringbone" structures, leaving a hollow tubular space in the central parts of CNTs.[66−69] The boundary crystal planes of the included metals are normally the {111} type owing to their thermodynamic stability and the structural conformation of adsorbed C_2H_2 on a 3-fold site during the carbon deposition.[66−69] Annealing at higher temperatures will lead to structural reconstructions of both metallic and CNTs phases.[69] It should be mentioned that more helical CNTs can be obtained using precursor β-Ni(OH)$_2$ in this reaction

(Figure 9e−g). In particular, the helical CNTs have been found to form favorably on the surfaces of the nickel spheres, and two different spiral directions are found (Figure 9h, FESEM image). Using the hollow spheres of NiO (reported in Figure 6), on the other hand, CNTs can also be grown onto the surface of the metal oxide, noting that the nickel atoms in the outermost surface region must have been reduced to metallic form (Ni_{surf}), in accordance to the reaction in eq 7. Nonetheless, compared to β-$Ni(OH)_2$, the reduction of NiO to metallic nickel is more difficult, and the basic structure of NiO can still be kept as demonstrated in Figure 10a (at 400 °C), while the CNTs phase is mainly produced as overlayers on the catalyst spheres under CNTs formation conditions at 450 °C [eq 8; Figure 10b−d]. Accordingly, less metal particles are included in the grown CNTs, although the helical form of CNTs can still be observed among the adjacent CNTs/NiO composite spheres (Figure 10d). In contrast, using porous nickel metals (reported in Figure 7) under the same reaction conditions, the Ni phase becomes hardly present (Figure 11a,b) and the product obtained in such a case is largely Ni@CNTs. Unlike the previous two cases, the C_2H_2 in the present reaction is exclusively for CNTs synthesis (not for Ni^{2+} reduction). Therefore, a greater reaction extent is expected. Indeed, many metallic droplets are trapped within the CNTs (Figure 11c). Interestingly, furthermore, the CNTs grown with the metal spheres are not helical, compared to the other two solid precursors (β-$Ni(OH)_2$ and NiO) discussed above.

$$\beta\text{-Ni(OH)}_2(s) + C_2H_2(g) \rightarrow Ni(s) + 2H_2O(g) + 2C_{CNTs}(s) \quad (5)$$

$$Ni(s) + nC_2H_2(g) \rightarrow Ni(s) + nH_2(g) + 2nC_{CNTs}(s) \quad (6)$$

$$NiO_{surf}(s) + C_2H_2(g) \rightarrow Ni_{surf}(s) + H_2O(g) + 2C_{CNTs}(s) \quad (7)$$

$$Ni_{surf}(s) + nC_2H_2(g) \rightarrow Ni(s) + nH_2(g) + 2nC_{CNTs}(s) \quad (8)$$

As a result of extruding puffy structures of hollow spheres of β-$Ni(OH)_2$, new secondary phases of materials can be easily deposited. Taking this structural advantage, for example, binary or ternary nanocomposites can be further prepared. In the work presented in Figure 12 (also refer to Figure 1), we introduced three different kinds of metal hydroxides onto the external surfaces of the β-$Ni(OH)_2$. In this preliminary exploration, the hydroxide flakes indeed can be inserted into the puffy (open) surfaces of the self-assembled hollow spheres. In Figure 12a,b, $Mg(OH)_2$ (brucite) flakes are deposited perpendicularly to the "petals" of β-$Ni(OH)_2$, while the basic structure of the β-$Ni(OH)_2$ sphere remain unaltered. In Figure 12c−f, similarly, β-$Co(OH)_2$ and $Fe(OH)_3$ are deposited respectively onto the β-$Ni(OH)_2$ phase. The presences of these secondary phases have been confirmed with our EDX analyses (Supporting Information, SI-4). Similar to those reported in Figures 6 and 7, in principle, the bihydroxide composites of this type can be used as precursor solids for preparations of even more complex nanocomposites of metal oxides and metals after respective thermal decomposition and reduction.

As depicted in Figure 1, the synthesis of self-assembled hollow spheres β-$Ni(OH)_2$ and the studied chemical conversions in liquid phase, solid state, and solid−gas reactions allow one to predict and synthesize a large set of Ni-containing nanomaterials with compositional design and structural architecture. With the present findings, exploration of this class of nanomaterials for their practical applications becomes the next immediate challenging research.

4. Conclusions

In summary, we have devised in this work a solution-based chemical approach to prepare hollow spheres of β-$Ni(OH)_2$, starting from thin flake nanobuilding units. It has been found that control of precipitation is a key to obtaining spherical porous morphology. Particularly, 6-coordinated nickel ion complex $[Ni(EDA)_3]^{2+}$ (EDA = $C_2H_4(NH_2)_2$) has been prepared as a nickel precursor to slow down the precipitation rate. By changing the starting concentration of divalent nickel in the precursor solutions, furthermore, the diameter of hollow spheres of β-$Ni(OH)_2$ can be controlled in submicrometer and micrometer regimes. The β-$Ni(OH)_2$ product spheres are constructed from petal-like flakes and platelets that are comprised of even smaller nanocrystallites in the size range of 3−4 nm. The thickness of the flakes/platelets along the *c*-axis of the β-$Ni(OH)_2$ crystal can be prepared in the range from 5 nm to a few tens of nanometers by varying the starting chemical concentrations. Under simple one-pot conditions, complex interior spaces (i.e., hollow and core−shell types of spheres) can be further attained. Typical specific surface area of β-$Ni(OH)_2$ hollow spheres has been determined at 93.2 m^2/g, and an unimodal pore-size distribution across a range of 2−5 nm has also been measured. During their self-assembly process, the hollow spheres of β-$Ni(OH)_2$ went through a donut type of structural intermediate. The as-synthesized β-$Ni(OH)_2$ spheres can be utilized as a solid precursor to synthesize other nanostructured derivatives. In this work, phase pure inorganic nanostructures, organic−inorganic nanocomposites, and inorganic−inorganic nanocomposites of NiO, Ni, NiO/Ni, Ni/β-$Ni(OH)_2$, CNTs/NiO, CNTs/Ni, Ni@CNTs, $Fe(OH)_3$/β-$Ni(OH)_2$, $Co(OH)_2$/β-$Ni(OH)_2$, and $Mg(OH)_2$/β-$Ni(OH)_2$ have been prepared via solid-state thermal decomposition, gas-phase reduction, solution-based reduction, surface oxidation, chemical vapor deposition, and liquid-phase deposition processes. Our efforts herein can be considered as the first attempt at a systematic investigation on nickel-related nanomaterials, and therefore a greater picture for the general chemical conversions of this materials family has been obtained.

(66) Audier, M.; Oberlin, A.; Coulon, M. *J. Cryst. Growth* **1982**, *57*, 524–534.
(67) Rodriguez, N. M.; Chambers, A.; Baker, R. T. K. *Langmuir* **1995**, *11*, 3862–3866.
(68) Chambers, A.; Rodriguez, N. M.; Baker, R. T. K. *J. Phys. Chem.* **1996**, *100*, 4229–4236.
(69) Feng, J.; Zeng, H. C. *J. Phys. Chem. B* **2005**, *109*, 17113–17119.

Acknowledgment. The authors gratefully acknowledge the financial support provided by the National University of Singapore, Singapore, and the King Abdullah University of Science and Technology, Saudi Arabia. S.M.Z. would also like to thank the China Scholarship Council (CSC) for providing his visiting scholarship at the National University of Singapore.

Supporting Information Available: HRTEM/TEM images and SAED patterns of β-Ni(OH)$_2$, NiO, and Ni/β-Ni(OH)$_2$ and EDX spectra of nanocomposites of Mg(OH)$_2$/β-Ni(OH)$_2$, Co(OH)$_2$/β-Ni(OH)$_2$, and Fe(OH)$_3$/β-Ni(OH)$_2$ (PDF). This material is available free of charge via the Internet at http://pubs.acs.org.

CM8028593